LRRC8A-containing chloride channel is crucial for cell volume recovery and survival under hypertonic conditions

Selma A. Serra[a,1], Predrag Stojakovic[b,c,1], Ramon Amat[b], Fanny Rubio-Moscardo[a], Pablo Latorre[b,c], Gerhard Seisenbacher[b,c], David Canadell[b,c], René Böttcher[b,c], Michael Aregger[d], Jason Moffat[d], Eulàlia de Nadal[b,c,2], Miguel A. Valverde[a,2], and Francesc Posas[b,c,2]

[a]Laboratory of Molecular Physiology, Department of Experimental and Health Sciences, Universitat Pompeu Fabra, 08003 Barcelona, Spain; [b]Department of Experimental and Health Sciences, Universitat Pompeu Fabra, 08003 Barcelona, Spain; [c]Institute for Research in Biomedicine, The Barcelona Institute of Science and Technology, 08028 Barcelona, Spain; and [d]Donnelly Centre, University of Toronto, Toronto, M5S 3E1 ON, Canada

Edited by Melanie H. Cobb, University of Texas Southwestern Medical Center, Dallas, TX, and approved May 6, 2021 (received for review December 12, 2020)

Regulation of cell volume is essential for tissue homeostasis and cell viability. In response to hypertonic stress, cells need rapid electrolyte influx to compensate water loss and to prevent cell death in a process known as regulatory volume increase (RVI). However, the molecular component able to trigger such a process was unknown to date. Using a genome-wide CRISPR/Cas9 screen, we identified *LRRC8A*, which encodes a chloride channel subunit, as the gene most associated with cell survival under hypertonic conditions. Hypertonicity activates the p38 stress-activated protein kinase pathway and its downstream MSK1 kinase, which phosphorylates and activates LRRC8A. LRRC8A-mediated Cl^- efflux facilitates activation of the with-no-lysine (WNK) kinase pathway, which in turn, promotes electrolyte influx via $Na^+/K^+/2Cl^-$ cotransporter (NKCC) and RVI under hypertonic stress. LRRC8A-S217A mutation impairs channel activation by MSK1, resulting in reduced RVI and cell survival. In summary, LRRC8A is key to bidirectional osmotic stress responses and cell survival under hypertonic conditions.

LRRC8A chloride channel | NKCC | p38/MSK1 | RVI | osmostress

The regulation of cell volume is essential for organism homeostasis (1). Cell swelling or shrinkage following osmotic stress exerts profound alterations of the cellular status (2), from short-term changes in the concentration of cell contents and signaling molecules (3) to modifications of the cell cycle (4, 5), transcription (6, 7), and chromatin organization (8). If not restored, such changes may cause cell death and pathological conditions, including neurological and epithelial alterations (9, 10). Cells have developed various mechanisms to rapidly regulate their volume when exposed to conditions that cause their shrinkage or swelling, the so-called regulatory volume increase (RVI) and regulatory volume decrease (RVD), respectively (1). When exposed to hypertonic environments, cells rapidly operate RVI mechanisms to preserve their functions and tissue survival (11). RVI involves electrolyte influx via the $Na^+/K^+/2Cl^-$cotransporter (NKCC) (12–15). NKCC activation was early associated to a reduced intracellular [Cl^-] (12, 14, 15) and the phosphorylation of the transporter (16). Later on, the role of the chloride-sensitive with-no-lysine (WNK) kinase pathway and its downstream targets in the activation of NKCC was identified (17–20). Na^+/H^+ and Cl^-/HCO_3^- exchangers working in parallel also cooperate to RVI (21). On the other hand, RVD mainly involves ion efflux through Cl^- (22, 23) and K^+ channels (24, 25), which respond to different intracellular signaling or mechanical cues triggered by cell swelling, or via K^+/Cl^- cotransporters also modulated by WNK (26). Therefore, most of the effectors participating in the regulation of cell volume are identified, but less is known about the mechanisms that initiate RVI. Recent evidence suggests direct osmosensing by the kinase domain of WNK due to a displacement of the equilibrium from a chloride binding conformation (inhibitory) to a low water availability (activating) conformation under high osmolarity conditions (27). In this model, reduction of the intracellular [Cl^-] may facilitate hyperosmotic-dependent activation of WNK and RVI, in line with reports from the early 1990s pointing to the link between low intracellular [Cl^-] and osmotically activated NKCC transport (12, 15). However, despite an intense search for the molecular pathways that regulate Cl^- movement across the plasma membrane when challenged by osmotic changes, there is still no answer for a question presented more than 30 y ago: How do cells maintain intracellular Cl^- at levels that facilitate WNK/NKCC activation and engage an effective RVI to protect them from death under hypertonic stress?

Results

LRRC8A Chloride Channel Favors Cell Survival under Hypertonic Conditions. To identify genes that are essential for cell survival upon hypertonicity, we conducted an unbiased loss-of-function genetic screen using the CRISPR-Cas9 system in HeLa cells infected with two libraries, each one containing around 90,000 guide RNAs (gRNAs) (28). Cells were grown for 6 d to discard essential genes. Then, cells were

Significance

Rapid regulatory volume increase (RVI) is important for cell survival under hypertonic conditions. RVI is driven by Cl^- uptake via the Na–K–Cl cotransporter (NKCC), which is activated by WNK kinases following a reduction in intracellular [Cl^-]. However, how intracellular [Cl^-] is regulated to modulate the WNK–NKCC axis and engage a protective RVI remains unknown. Our work reveals that LRRC8A-containing chloride channel is a key protective factor against hypertonic shocks. Considering that LRRC8A (SWELL1) is typically activated by low ionic strength under hypotonic stress, our results posed another interesting question: what activates this chloride channel under hypertonic stress? We demonstrated that, upon hyperosmotic activation, the p38-MSK1 pathway gates LRRC8A-containing chloride channel to facilitate activation of WNK–NKCC and an effective RVI.

Author contributions: S.A.S., P.S., R.A., F.R.-M., G.S., D.C., M.A., J.M., E.d.N., M.A.V., and F.P. designed research; S.A.S., P.S., R.A., F.R.-M., G.S., D.C., and M.A. performed research; S.A.S. and P.S. contributed new reagents/analytic tools; S.A.S., P.S., P.L., R.B., J.M., E.d.N., M.A.V., and F.P. analyzed data; and S.A.S., P.S., F.R.-M., P.L., J.M., E.d.N., M.A.V., and F.P. wrote the paper.

The authors declare no competing interest.

This article is a PNAS Direct Submission.

See online for related content such as Commentaries.

[1]S.A.S. and P.S. contributed equally to this work.

[2]To whom correspondence may be addressed. Email: eulalia.nadal@irbbarcelona.org, miguel.valverde@upf.edu, francesc.posas@irbbarcelona.org.

This article contains supporting information online at https://www.pnas.org/lookup/suppl/doi:10.1073/pnas.2025013118/-/DCSupplemental.

Published June 3, 2021.

subjected to hypertonic conditions for 24 h (+150 mM NaCl) (Fig. 1*A*). *LRRC8A*, which encodes for a subunit of a swelling-activated chloride channel (29, 30), was the gene most associated with increased hypertonicity-induced cell death (Fig. 1*B* and *SI Appendix*, Table S1 and Fig. S4). The use of a crystal violet assay or propidium iodide (PI) staining to quantify cell viability in several cell lines exposed to the specific LRRC8A channel inhibitor 4-(2-butyl-6,7-dichloro-2-cyclopentylindan-1-on-5-yl)oxybutyric acid (DCPIB) (31) confirmed the role of LRRC8A in cell survival under hypertonic conditions (Fig. 1 *C* and *D* and *SI Appendix*, Fig. S1 *A*–*C*). Notably, cell death almost doubled in those cells exposed to DCPIB and extracellular hypertonicity. The involvement of LRRC8A in the protection against hypertonicity-induced cell death was also validated in HeLa-LRRC8A-KO (knock-out) cells engineered using the CRISPR technique (Fig. 1*D* and *SI Appendix*, Fig. S1*D*).

The LRRC8A Cl^- channel is activated in response to low ionic strength (IS) following cell swelling (32–34). Thus, we tested whether LRRC8A preserved this function in our HeLa model. A swelling-activated Cl^- current with higher permeability to I^- than to Cl^- has been reported in HeLa cells (35). In KO and HeLa cells transfected with small interfering RNA (siRNA) against LRRC8A, the activity of a swelling-activated chloride channel sensitive to DCPIB and tamoxifen (36) was reduced compared to control LacZ cells (LZ), as shown by electrophysiological experiments (*SI Appendix*, Fig. S2 *A* and *B*), quenching of the fluorescence signal caused by I^- influx into cells expressing the halide-sensitive yellow fluorescent protein (YFP) (29, 30, 37) (*SI Appendix*, Fig. S2 *C* and *D*), and RVD analysis (*SI Appendix*, Fig. S2 *E* and *F*). These observations thus confirm the defined role of LRRC8A as a necessary subunit of the swelling-activated chloride channel in these cells.

Our finding that LRRC8A, in addition to its role in the cellular response to swelling, is also involved in protecting cells against hypertonicity-induced cell death was unexpected and defied our current understanding of LRRC8A regulation by low IS and the mechanisms that cells activate to respond to volume changes. To decipher how LRRC8A is involved in the response to hypertonicity, we first measured the quenching of YFP in intact cells. Exposure to hypertonic conditions activated a plasma membrane Cl^- conductance, which became apparent when cells were perfused with NaI, and the YFP signal decreased (Fig. 1 *E* and *F*). YFP quenching was significantly reduced in KO cells. A similar reduction in YFP quenching was obtained by downregulating LRRC8A with siRNA (*SI Appendix*, Fig. S3 *A* and *B*), following channel inhibition with tamoxifen (*SI Appendix*, Fig. S3 *C* and *D*) or DCPIB (*SI Appendix*, Fig. S3 *E* and *F*). Furthermore, we observed an increase in LRRC8A whole-cell chloride currents sensitive to DCPIB in control LZ compared to KO cells bathed in hypertonic solutions and dialyzed with low IS hyperosmotic solutions (Fig. 1 *G* and *H*).

LRRC8A Is Regulated upon Hypertonicity by the p38/MSK1 Kinase Pathway. We next investigated how the chloride channel activity was induced under hypertonic conditions. p38 SAPK is known to be activated by hyperosmolarity (38) and to mediate cell adaptation in hypertonic conditions (2, 38). We observed p38 phosphorylation (indicative of its activation) after a hypertonic challenge in both LZ and KO cells (*SI Appendix*, Fig. S4*A*). Notably, activity of LRRC8A-containing channels under hypertonic conditions was reduced by the p38 inhibitor SB203580 (39) (Fig. 2*A*) and in p38α-KO cells (*SI Appendix*, Fig. S4*B*), consistent with a channel gating mechanism involving the p38 pathway. Genetic inhibition of p38α did not affect chloride channel activation under hypotonic conditions (*SI Appendix*, Fig. S4*C*).

LRRC8A was phosphorylated under hypertonic conditions but not in HeLa-p38α-KO cells (*SI Appendix*, Fig. S4*D*). However, no phosphorylation sites sensitive to the p38 inhibitor SB203580 were detected in residues of LRRC8A that are exposed intracellularly. Therefore, we focused on the mitogen- and stress-activated kinase 1 (MSK1), a downstream kinase directly regulated by p38 (40). Exposure to hyperosmotic shocks likewise triggered MSK1 phosphorylation (*SI Appendix*, Fig. S4*E*). MSK1 is primarily a nuclear kinase that also shuttles to the cytosol upon hypertonic stress (*SI Appendix*, Fig. S4*F*). Strikingly, inhibition of MSK1 with SB747651A (41) prevented LRRC8A phosphorylation in response to hyperosmotic stress (Fig. 2*B*) and, similar to p38 inhibition, decreased the level of LRRC8A activity (Fig. 2*A*). Next, we focused on identifying the LRRC8A residue(s) required for MSK1-mediated phosphorylation and activation under hypertonic conditions. LRRC8A contains several putative MSK1 phosphorylation sites (Fig. 2*C*). The intracellular loop (ICL) of LRRC8A was strongly phosphorylated in vitro by MSK1, and the mutation of Serine 217 to Alanine (S217A) almost completely abolished MSK phosphorylation in this region (Fig. 2*D*) and in the full-length LRRC8A (Fig. 2*E*). We next measured chloride currents in HeLa cells in which *LRRC8A* expression was stably knocked down by small interfering RNA (shRNA) (KD) (29) and overexpressed LRRC8A-wild type (WT) or LRRC8A-S217A (shRNA resistant). Indeed, LRRC8A-WT but not LRRC8A-S217A–expressing cells generated Cl^- currents after dialysis in low IS solutions and exposure to hypertonic conditions (Fig. 2*F*). We then examined whether genetic activation of MSK1 leads to LRRC8A activation in the absence of any osmotic stress or change in IS. Expression of a constitutively active MSK1 (MSK1-T581D+T700D) (42) spontaneously activated a DCPIB-sensitive Cl^- current in KD cells overexpressing LRRC8A-WT but not in those cells overexpressing LRRC8A-S217A channels (Fig. 2*G*). Thus, we demonstrate that activation of the p38/MSK1 pathway under hyperosmotic conditions is sufficient to activate LRRC8A even without changes to the intracellular IS.

LRRC8A Facilitates the WNK/NKCC Axis to Support RVI and Cell Survival. We hypothesized that MSK1-mediated activation of LRRC8A under hypertonic conditions provides a pathway for Cl^- efflux that contributes to the activation of NKCC, and therefore, we addressed how LRRC8A participates in the cell volume response to hypertonic stress. Following exposure to hypertonic stress, shrunken cells immediately react by activating a rapid uptake of electrolytes via NKCC and the osmotically obliged water, thereby regaining the initial cell volume (1). Reports on the need to reduce intracellular $[Cl^-]$ to trigger NKCC activity (12, 15) and the Cl^--dependent phosphorylation of NKCC date back to the 1990s (16, 43, 44), but no molecular mechanism has been proposed to date as how intracellular $[Cl^-]$ is reduced in the face of hypertonic conditions. By measuring RVI after hypertonic cell shrinkage, we found that cell volume rapidly shrunk by 30% under hypertonic conditions in both LZ and LRRC8A-KO cells (Fig. 3*A*). Cell shrinkage was followed by a slow increase in volume toward initial values, quantified as the cell volume recovered from the maximum shrinkage (% RVI). LZ cells reached ~40% RVI (Fig. 3*B*). In contrast, KO (Fig. 3 *B* and *C*) and p38α-KO cells (Fig. 3*C*) showed a marked reduction in RVI, similar to cells treated with DCPIB or with the inhibitors of p38 or MSK1 (Fig. 3*D*). The different RVI response between LZ and KO cells cannot be attributed to differences in the basal cell volume (*SI Appendix*, Fig. S5*A*) or initial hypertonicity-induced shrinkage (*SI Appendix*, Fig. S5*B*) as both parameters did not differ between LZ and KO cells. RVI was also impaired in KD cells overexpressing the shRNA-resistant LRRC8A-S217A mutant, in contrast to cells overexpressing LRRC8A-WT, which showed a significant increase in RVI (Fig. 3*E*).

The NKCC inhibitor bumetanide (45) prevented RVI in LZ cells but not in KO cells (Fig. 3*F*), showing that the final effector responsible for increased RVI downstream of LRRC8A was the NKCC triple cotransporter. The involvement of LRRC8A in the activation of NKCC was also evaluated by measuring the halide-dependent quenching of YFP tagged to the intracellular side of NKCC1 (46). HeLa cells transfected with YFP-tagged NKCC1

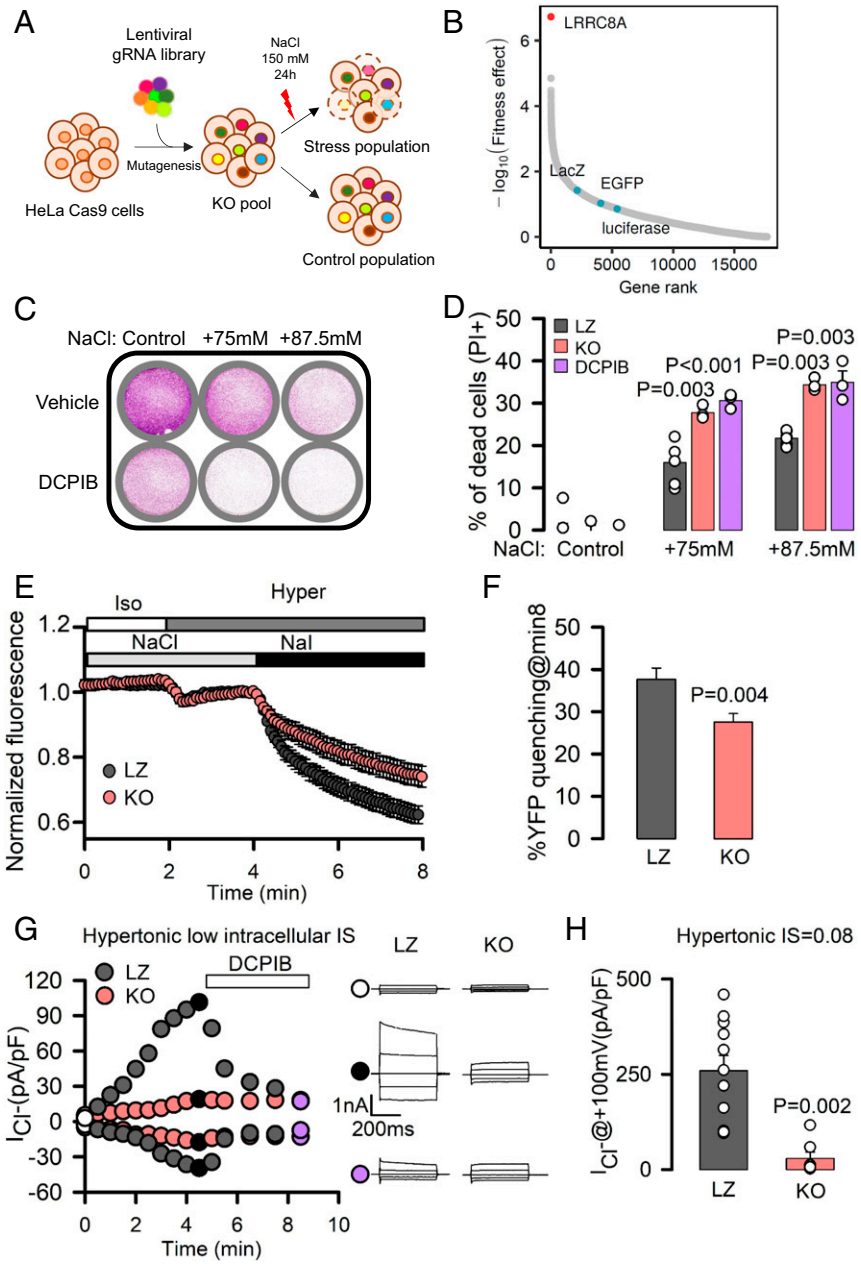

Fig. 1. LRRC8A activation is essential for cell fitness upon hypertonicity. (*A*) Schematic diagram of unbiased CRISPR/Cas9 genome-wide genetic screening to identify genes relevant for adaptation to high osmolarity. (*B*) Representation of the MAGeCK per-gene fitness effect score ($-\log_{10}$ RRA score). A higher fitness effect indicates a higher degree of importance for cell viability upon hyperosmotic stress. Gene name of LRRC8A is indicated, together with the name of nontargeting controls (LacZ, EGFP, luciferase, blue dots). (*C* and *D*) Crystal violet staining or PI staining (to monitor cell death) of LZ, LRRC8A-KO, and HeLa cells treated with DCPIB and exposed to different doses of hypertonic stress. *P* values determined by one-way ANOVA followed by post hoc Dunnett's test versus LZ control group. (*E*) Mean ± SEM. YFP fluorescence changes (normalized to the baseline in isotonic conditions) in LZ and KO HeLa cells transiently transfected with halide-sensitive YFP. Addition of isotonic and hypertonic bathing solutions containing NaCl or NaI is indicated by boxes at the top of the recordings. (*F*) Percentage of YFP quenching measured 8 min after the addition of NaI. Mean ± SEM (LZ, $n = 66$; KO, $n = 59$). *P* values were determined by two-tailed Student's *t* test. (*G*) Time course of whole-cell chloride currents recorded at –100 mV and +100 mV in LZ (gray) and KO (red) HeLa cells dialyzed with hyperosmotic solutions with an IS of 0.08 and then exposed to hypertonic solutions followed by exposure to 36 μM DCPIB. (*Right*) Families of chloride currents measured at the points indicated in the *Left*. Cells here held at 0 mV and pulsed from –100 mV to +100 mV in 50-mV steps. (*H*) Maximal mean current densities measured in LZ and KO HeLa cells under the experimental conditions shown in *G*. *P* values determined by Student's *t* test.

showed a decrease in the intensity of the YFP signal when challenged with hypertonic solutions (due to Cl^- entry via NKCC). Quenching was prevented in the presence of DCPIB or the NKCC inhibitor azosemide (45) (*SI Appendix*, Fig. S6 *A* and *B*). Taken together, RVI results obtained from both cell models (KO and KD cells) indicate that LRRC8A activation downstream of p38/MSK1 provides a pathway for Cl^- efflux and signals the triple cotransporter to take up electrolytes, thereby ensuring efficient RVI. If this mechanistic model is correct, imposing reduced intracellular [Cl^-] should overcome the deficient functional coupling of the LRRC8A and NKCC1 transport systems in LRRC8A-KO cells and ensure efficient RVI. To test this, we exposed cells to a hypotonic shock (to increase their volume and to reduce intracellular ion concentrations) followed by a return to isotonic

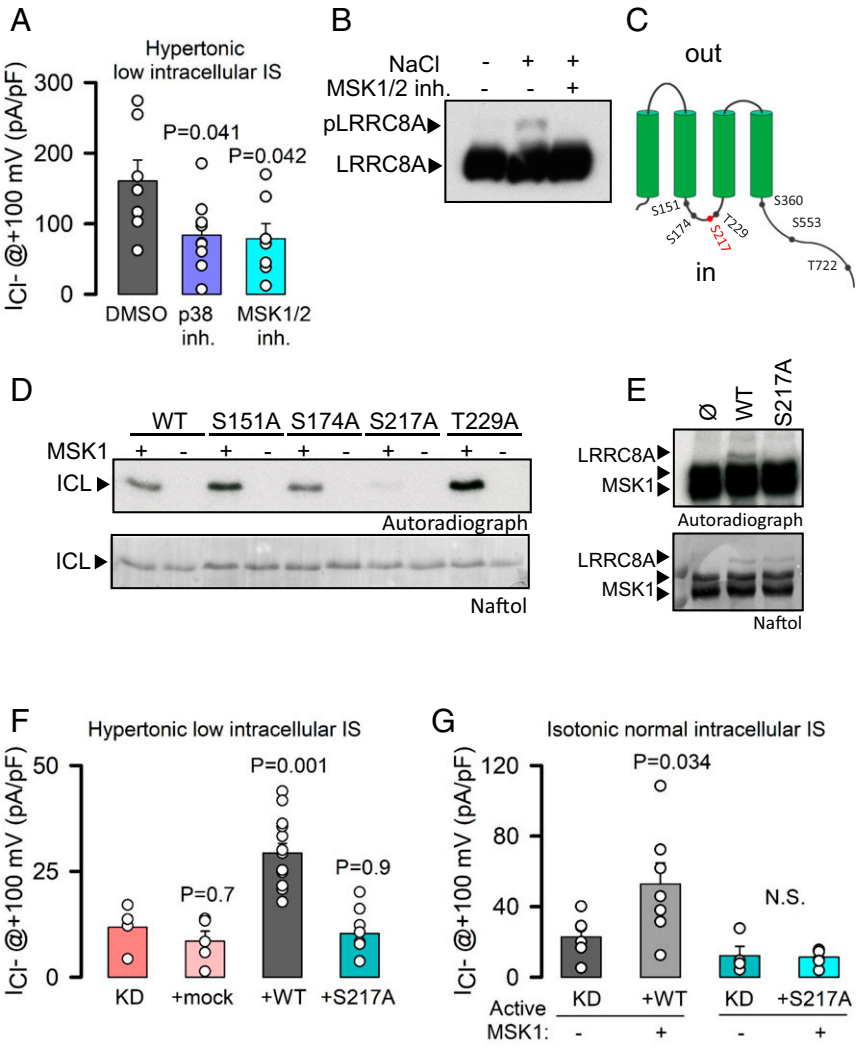

Fig. 2. The p38/MSK1 pathway regulates LRRC8A activation upon hypertonicity. (*A*) Maximal mean current densities (±SEM) measured in LZ and KO HeLa cells dialyzed with hyperosmotic solutions of 0.08 IS and exposed to hypertonic solutions containing DMSO (0.1%), the p38 inhibitor (SB203580, 10 μM), or the MSK1 inhibitor (SB747651A, 10 μM). *P* values were determined by one-way ANOVA followed by post hoc Dunnett's test versus a DMSO control group. (*B*) Western blot analysis of LRRC8A in a Phos-tag gel of extracts obtained from HeLa cells exposed to hypertonic (+100 mM NaCl) solutions in the absence or presence of SB747651A. (*C*) Schematic diagram of MSK1 phosphorylation sites in LRRC8A. (*D*) In vitro phosphorylation by MSK1 of the ICL (amino acids 144 to 258) of LRRC8A-WT as well as of single mutants. (*E*) In vitro phosphorylation of full-length LRRC8A-WT and LRRC8A-S217A by MSK1. (*F*) Maximal mean current densities (±SEM) measured in stable LRRC8A KD HeLa cells overexpressing shRNA-resistant LRRC8A-WT or LRRC8A-S217A. Cells were dialyzed with hyperosmotic solutions with an IS of 0.08 and exposed to hypertonic solutions. *P* values were determined by one-way ANOVA followed by post hoc Dunnett's test versus KD control group. (*G*) Maximal mean current densities (±SEM) measured in KD HeLa cells recorded under control isotonic conditions. Cells overexpressed shRNA-resistant WT or S217A LRRC8A with or without coexpression of a constitutively active MSK1 (MSK1-T581D/T700D). *P* values were determined by Student's *t* test comparing the effects of MSK1 expression on WT or mutant channel.

conditions, at which point cells shrink as a result of increased osmolarity and the efflux of water. This maneuver has been classically used for the preactivation of NKCC to achieve an efficient RVI in cells that do not up-regulate cell volume when challenge with hypertonic conditions (1, 14). In response to this treatment, cells typically engaged first in RVD, followed by RVI on returning to isosmotic conditions (Fig. 3*G*). KO cells presented reduced RVD because of impaired LRRC8A-mediated Cl^- efflux (see also *SI Appendix*, Fig. S2*E*) but similar RVI to that of LZ cells (Fig. 3*H*). Under these conditions of reduced intracellular [Cl^-] due to previous hypotonic cell swelling, NKCC activation was favored, and both LZ and KO cells attained equally efficient RVI, even in the absence of LRRC8A, suggesting that disparities in the intracellular levels of Cl^- between LZ and KO cells may underlie the differences in RVI.

To understand the link between LRRC8A and NKCC activities, we focused on WNK kinases. The ubiquitously expressed WNK1 is autophosphorylated and activated by a reduction in intracellular [Cl^-], triggering its downstream targets SPAK and OSR1 kinases, which ultimately phosphorylate and activate NKCC1 (17–20, 47). WNK1 showed a reduced activation (measured using an anti–phosho-WNK-S382) in KO and KD cells when compared to LZ cells exposed to hypertonic solutions (Fig. 4*A* and *SI Appendix*, Fig. S7 *A* and *B*). However, WNK1 phosphorylation was not different between LZ and KO cells exposed to the isotonic-hypotonic-isotonic protocol shown in Fig. 3*G* (Fig. 4*B*); this is consistent with our data showing that experimental reduction of intracellular [Cl^-] by previous exposure to hypotonic solutions improved the RVI of KO cells to the level of LZ cells. These results also suggest that LRRC8A-driven RVI regulation occurs upstream of the activation of the

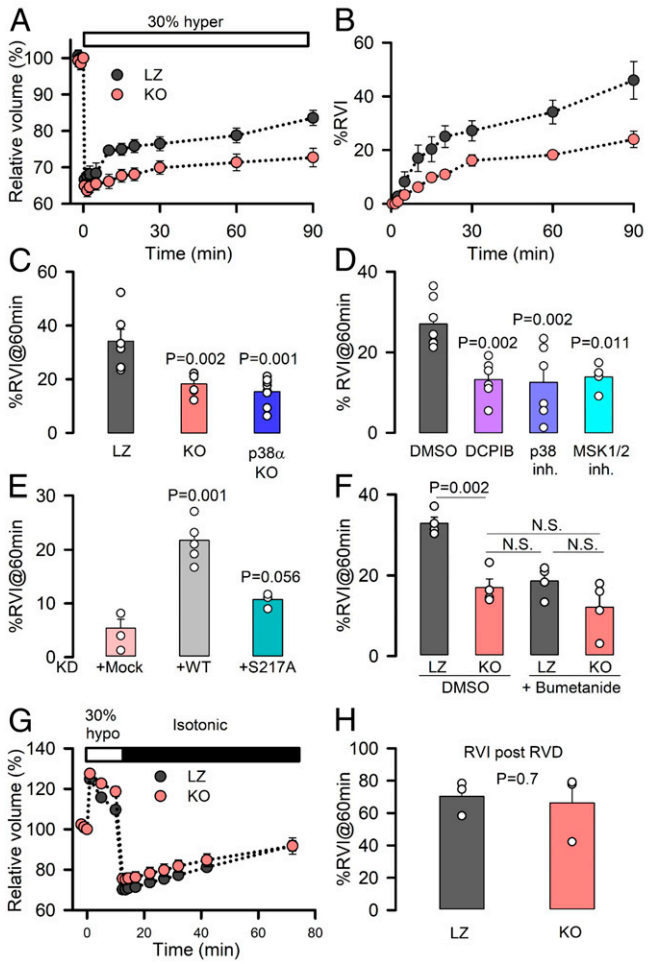

Fig. 3. The p38/MSK1 pathway and LRRC8A regulate NKCC-mediated RVI. (*A*) Time course of relative changes in cell volume of LZ and KO HeLa cells (normalized to isotonic conditions) before and after exposure to a 30% hypertonic medium. Mean ± SEM ($n = 6$). (*B*) Percentage of RVI, calculated as the percentage of volume recovered following the initial cell shrinkage at the different time points after the hypertonic stress. (*C*) Mean RVI (%) calculated at 60 min in LZ ($n = 6$), KO ($n = 6$), or p38α-KO ($n = 9$) HeLa cells. (*D*) Mean RVI (%) calculated at 60 min in HeLa cells superfused with DMSO ($n = 7$), the LRRC8A channel inhibitor DCPIB ($n = 6$), the p38 inhibitor SB203580 ($n = 6$), or the MSK1 inhibitor SB747651A ($n = 4$). (*E*) Mean RVI (%) calculated at 60 min in KD ($n = 4$) HeLa cells overexpressing shRNA-resistant WT ($n = 6$) or S217A ($n = 4$) LRRC8A channels. (*F*) Mean RVI (%) calculated at 60 min after LZ or KO HeLa cells were exposed to DMSO or 50 μM bumetanide. (*G*) Relative changes in cell volume measured before and after superfusion of LZ or KO HeLa cells with a 30% hypotonic medium. (*H*) Mean RVI (%), generated after RVD, was calculated at 60 min after return to isotonic medium, as shown in *G* ($n = 3$). *P* values were determined by two-tailed Student's *t* test (*H*), a Bonferroni's all pairwise comparison (*F*), or one-way ANOVA followed by post hoc Dunnett's test versus control group (*Left Bar*) (all others).

WNK1–NKCC1 axis. To further confirm the link between LRRC8A-containing Cl^- channels and WNK1 activation, first, we overexpressed shRNA-resistant LRRC8A in KD cells and demonstrated that, unlike mock, overexpression of LRRC8A rescued WNK1 phosphorylation in response to hypertonic stimulation (*SI Appendix*, Fig. S7 *C* and *D*). Second, for LRRC8A-mediated efflux of Cl^- to regulate WNK1 activation, the change in intracellular [Cl^-] should occur at very early stages of the cell response to hypertonic conditions. We addressed this point by measuring intracellular [Cl^-] in cells overexpressing the GFP-based ratiometric Cl^- sensor ClopHensor (48) (*SI Appendix*, Fig. S8 *A* and *B*) or loaded with the Cl^- sensitive fluorescent dye MQAE (*SI Appendix*, Fig. S8*C*). Following exposure to hypertonic solutions, both LZ and KO cells showed a reduction in the fluorescence signal (indicating increased [Cl^-]) due to cell shrinkage. However, while LZ cells rapidly increased the fluorescence signal (because of reduction in intracellular [Cl^-]), KO cells did not reduce intracellular [Cl^-] and maintained a decreased signal, thereby supporting the role of LRRC8A-mediated channels in the modulation of WNK1 by affecting intracellular [Cl^-]. The involvement of WNK1 in the regulation of RVI by LRRC8A-containing Cl^- channels was also assessed by transfecting LZ and KO cells with inactive WNK1-S382A or kinases that are constitutively active (17, 18) by mutating the phosphorylatable Ser382 (WNK1-S382E) or making the kinase Cl^- insensitive and increasing its autophosphorylation (WNK1-L369F/L371F) (*SI Appendix*, Fig. S9). WNK1-S382E or WNK1-L369F/L371F overexpression, but not WNK-S382A, rescued RVI in KO cells, whereas none affected RVI levels in LZ cells (Fig. 4*C*).

Finally, we studied cell survival under hypertonic conditions in KO cells expressing inducible LRRC8A-WT (KO-iWT) or LRRC8A-S217A (KO-iS217A) proteins to levels similar to those found in control HeLa cells (*SI Appendix*, Fig. S10*A*). Expression of iWT but not iS217A increased cell survival to levels comparable with LZ cells (Fig. 4*D*). Similarly, transfection of KD cells with shRNA-resistant LRRC8A-WT and LRRC8A-S217A channels resulted in increased survival of LRRC8A-WT– but not LRRC8A-S217A–expressing cells under hypertonic conditions (*SI Appendix*, Fig. S10*B*).

Discussion

Our work unexpectedly reveals that swelling-activated chloride channels containing the LRRC8A subunit are also critical for cell survival under hypertonic conditions. Based on a genome-wide CRISPR/Cas9 screen, KO cell models, cell imaging, electrophysiological, and pharmacological and molecular tools, we demonstrate that LRRC8A works as a bidirectional osmotic stress response element: as a Cl^- efflux pathway that favors loss of electrolytes during RVD, and as a regulator of the Cl^--sensitive WNK–NKCC axis to activate gain of electrolytes during RVI. Our results also reinforce the recent view about the role of LRRC8A-containing channels in cell responses to stresses other than cell swelling (49) and confirm the link between the need for correct RVI regulation and increased cell fitness in the face of hypertonic stress (11). We propose a mechanism (Fig. 4*E*) by which activation of the p38/MSK1 pathway phosphorylates and activates the LRRC8A chloride and promotes Cl^- efflux, which in turn facilitates shifting the conformational equilibrium of WNK1 from the chloride-bound inhibitory state toward the less-hydrated, active state triggered by hypertonicity (27). Thus, the combination of both direct activation of WNK1 by hyperosmotic stress and reduction in Cl^--mediated autoinhibition may represent a mechanism to ensure optimal WNK1 activation and guarantee NKCC1-mediated transport to promote RVI and cell survival in response to hypertonic environments. Numerous reports over the last 30 y have documented the activation of NKCC by cell shrinkage and/or reduction in intracellular [Cl^-] (reviewed by refs. 1 and 14). The identification of the chloride-sensitive WNK and its downstream phosphorylation pathway resulting in NKCC phosphorylation resolved how NKCC is activated by low intracellular [Cl^-], whereas the mechanisms by which the WNK–NKCC axis is activated under hypertonic conditions have remained elusive until recently. The Cl^- hypothesis of NKCC activation seems counterintuitive in the face of increased intracellular [Cl^-] triggered by cell shrinkage. However, it has been shown that cell shrinkage modifies the sensitivity of the WNK–NKCC axis to Cl^-, introducing a 20-mM right shift in the Cl^- dependence of the transporter (15, 16) and postulated that decreases in intracellular [Cl^-] from its elevated hypertonicity-induced set point may participate in the activation of NKCC (16). Therefore, activation of LRRC8A under hypertonic conditions may

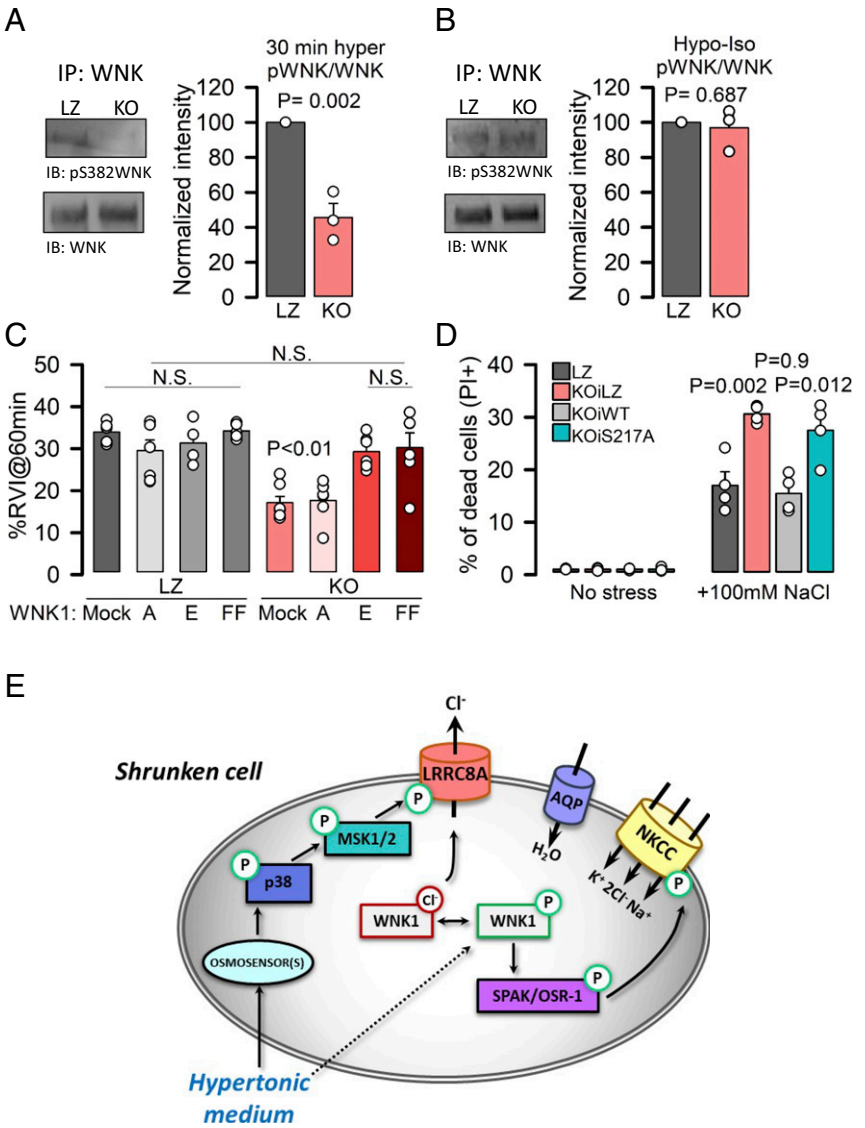

Fig. 4. LRRC8A triggers WNK activation to promote RVI and cell survival under hypertonicity. (*A*) Phosphorylation of immunoprecipitated WNK1 obtained from cell lysates of LZ and KO HeLa cells exposed to 30% hypertonic medium. (*Left*) Western blot of p-S382 and total WNK1; (*Right*) quantification of phosphorylated WNK1 (normalized to total immunoprecipitated WNK1) after 30-min exposure to hypertonic medium. *P* values were determined by two-tailed Student's *t* test ($n = 3$). (*B*) Western blot and quantification of p-S382 WNK1 of immunoprecipitates obtained from cell lysates of LZ or KO HeLa cells ($n = 3$) in an isotonic medium after exposure to 30% hypotonic medium (as described in Fig. 3*G*). (*C*) Mean (±SEM; $n = 4$ to 7) RVI (%) calculated at 60 min in LZ or KO HeLa cells overexpressing mock, WNK1-S382A (A), WNK1-S382E (E), or WNK1-L369F/L371F (FF). *P* values were determined by all pairwise one-way ANOVA followed by Holm–Sidak post hoc test. $P < 0.01$ only when comparing KO mock or KO WNKA with any other condition. (*D*) PI staining (to monitor cell death) of KO cells expressing WT or S217A mutant LRRC8A under an inducible promoter (DOX). (*E*) Model of the mechanism that links the p38/MSK1 phosphorylation pathway with the WNK1–NKCC1 axis via LRRC8A to promote RVI and cell survival in response to hypertonic environments.

prevent excessive increase in intracellular [Cl^-], maintaining a level that although elevated compared to isotonic conditions optimizes WNK1 activation by hypertonic stimuli. Indeed, our results showing that genetic inhibition of LRRC8A reduced WNK1 phosphorylation and efficient RVI (also impaired using LRRC8A channel inhibitors) support the hypothesis that hypertonicity-induced activation of the WNK–NKCC axis is modulated by a reduction in intracellular [Cl^-]. Further support to the relevance of intracellular Cl^- on WNK–NKCC axis activation under cell shrinkage conditions came from experiments in which intracellular [Cl^-] was previously reduced by exposing cells to a hypotonic shock (Fig. 3 *G* and *H* and Fig. 4*B*) or by overexpressing a Cl^--insensitive WNK1 (Fig. 4*C* and *SI Appendix*, Fig. S9). Under these conditions, no differences in WNK1 phosphorylation or RVI were observed between LZ and KO cells, thereby suggesting that the effect of LRRC8A-containing channels on the modulation of the WNK1–NKCC axis is through the modulation of intracellular Cl^- concentrations. Actually, direct activation of the purified kinase domain of WNK by osmolytes is promoted by reducing [Cl^-] (27), in concordance with our findings that LRRC8A-mediated Cl^- efflux prevents excessive accumulation of intracellular Cl^- and promotes WNK1–NKCC activation in intact cells.

Despite the numerous experimental approaches used for the demonstration of the involvement of LRRC8A in the cell response to hypertonicity, our study is not exempt of limitations. One is the technical difficulty to directly record channel activity in the transition from isotonic to hypertonic conditions with a recording pipette attached to the cell membrane. Also, we cannot completely rule out that channel activation in response to hypertonic stress is solely mediated by MSK1-mediated phosphorylation, without

involving changes in IS or other possible modulators that are triggered in response to hypertonic stress. Nevertheless, our results expressing active MSK1 as well as LRRC8A-S217A mutants pointed to MSK1-mediated phosphorylation being the main mechanism for channel activation in the absence of changes in intracellular IS. Related to this, classical activation of LRRC8A-type chloride channels is known to depend on the presence of intracellular ATP and the rate of cell swelling (50–52), being more relevant with small changes in IS and less relevant with rapid and larger changes in IS. This is consistent with the involvement of an ATP-dependent phosphorylation event in the gating of LRRC8A-containing chloride channels in the face of small changes in IS.

Our data also shows that LRRC8A links two phosphorylation pathways (p38/MSK1 and WNK1) participating in the cell response to osmotic stress and invites a review of the role of LRRC8A in different pathophysiological conditions involving WNK (53) or MSK1 signaling (54, 55).

Materials and Methods

Drugs, antibodies, oligonucleotides, and plasmids used are described in *SI Appendix*, Table S2.

Genetic Screening and Analysis. To identify genes that are essential for hypertonic stress survival, an unbiased loss-of-function genetic screening was performed in HeLa cells using the CRISPR-Cas9 system (28). Cells expressing a constitutive hCas9 were infected with one of two lentiviral gRNA libraries ([Toronto KnockOut Library] TKO-1 or TKO-2) (28). Cells were selected by adding puromycin (1.5 μg/mL) at 24-h postinfection, and multiplicity of infection (MOI) was determined after 48 h (T0) by comparison with nonselected infected cells (TKO-1, MOI = 0.34; TKO-2, MOI = 0.5). At this point, 20×10^6 cells were collected for subsequent genomic DNA (gDNA) extraction and sequencing to ensure good library representation (T0). The rest of the cells were split into three replicates (A, B, and C), each covering a 200-fold representation of each library (20×10^6 cells). Cells were then split every 3 d, always keeping a 200-fold representation of each library. At T6, cells were seeded and 24 h later were challenged with hypertonic stress (150 mM NaCl) or kept in regular medium. One day after, they were counted and frozen (20×10^6 cells) for subsequent gDNA extraction, library preparation, and next generation sequencing, which were carried out as in ref. 28. Briefly, genomic DNA was extracted from cell pellets using the QIAamp Blood Maxi Kit (Qiagen). gRNA inserts were amplified via PCR using primers harboring Illumina TruSeq adapters with i5 and i7 barcodes, and the resulting libraries were sequenced on an Illumina HiSeq2500. Each read was completed with standard primers for dual indexing with Rapid Run V1 reagents. The first 20 cycles of sequencing were "dark cycles" or base additions without imaging. The actual 26-base pairs read began after the dark cycles and contained two index reads, reading the i7 sequences first, followed by i5.

Model-based Analysis of Genome-wide CRISPR-Cas9 Knockout (MAGeCK) (56) was used to evaluate the quality of screening data and to identify osmostress fitness genes. MAGeCK is specifically designed to analyze genome-wide CRISPR-Cas9 screenings, and it computes a per-gene fitness effect score by integrating information from all sgRNAs targeting a given gene. This so-called robust rank aggregation (RRA) score indicates the degree of selection of a gene in a screening. Correct establishment of the KO library is a proxy for good quality of the screening. An efficiently established library should be depleted of genes essential for cell survival. For this reason, both day 8 control cells and NaCl-treated cells were compared against day 0 libraries using MAGeCK. Genes were then ranked by RRA, and a gene set enrichment analysis (GSEA) (57) was performed against the entire Kyoto Encyclopedia of Genes and Genomes (KEGG) database (*SI Appendix*, Table S3). As expected, essential terms were enriched among the top depleted genes (false discovery rate [FDR] < 0.01) (including RNA polymerase, proteasome, spliceosome, cell cycle, and ribosome), thereby proving the correct establishment of our KO libraries. Next, day 8 control and NaCl-treated cells were compared using MAGeCK to identify genes whose KO causes defects in cell proliferation upon hyperosmotic stress (*SI Appendix*, Table S4). After multiple testing correction using the Benjamini–Hochberg procedure, LRRC8A/SWELL1 emerged as the top scoring candidate (Fig. 1*B*; rank 1, FDR = 0.064).

Quality control of reads and mapping. Raw sequencing reads from CRISPR-Cas9 samples were assessed for quality using FASTQC (version [v]0.11.5) and subsequently aligned to the sgRNA sequences of the TKO (28) (available at http://tko.ccbr.utoronto.ca/) using BowTie (v1.2.1.1; parameters used: –m 1 –v 2) (58). Read counts for each sgRNA were tabulated and used for downstream analyses.

Quality control of the screening and identification of fitness genes. Downstream analyses were performed using MAGeCK (v0.5.6) (https://sourceforge.net/p/mageck/wiki/Home/) (56). GSEA for quality control of the screening (Day 0 versus Day 8 comparison) was done with MAGeCK's "pathway" command, with default parameters, using KEGG pathways (v6.0) from the Molecular Signatures Database (https://www.gsea-msigdb.org/gsea/msigdb/collections.jsp) (59) as input. Candidate fitness genes for hyperosmotic stress were identified using MAGeCK's "test" command with default parameters (*SI Appendix*, Table S4). In both cases, the whole TKO library, comprising two sublibraries (base and *SI Appendix*), was used. Both sublibraries were normalized to the median ratio (MAGeCK's default), merged into a single library, and analyzed with MAGeCK's "test" command without further normalization (-norm-method none).

Cell Lines. Cells were maintained in Dulbecco's Modified Eagle's Medium (Gibco) containing 10% fetal calf serum (Sigma) supplemented with 1 mM sodium pyruvate and 100 U/mL penicillin (Gibco) and cultured in a 5% CO_2 humidified incubator at 37 C. HeLa cells (human, cervical epithelial, female) were purchased from the American Type Culture Collection and HeLa cells stably expressing Cas9, from ref. 28. HeLa-shLRRC8A cells (KD) were kindly provided by Dr. A. Patapoutian, Department of Neuroscience, The Scripps Research Institute, La Jolla, CA (29).

Control HeLa Cas9 LZ cells, LRRC8A-KO (KO) cells, p38-KO cells, and HeLa Cas9 LRRC8A-KO clone 6 cells expressing LRRC8A-WT (KO-iWT) or LRRC8A-S217A (KO-iS217A) under an inducible promoter were generated as described below. gRNA targeting *LacZ* or *KOs* from the TKO-1 library (see gRNAs sequences; *SI Appendix*, Table S2) were cloned into the pLCKO vector. To produce lentiviruses, guidelines of the "The RNAi Consortium" at the Broad Institute (https://portals.broadinstitute.org/gpp/public/resources/protocols) were followed. Briefly, 60 to 70% confluent 293T cells were transfected with pLCKO together with packing vectors (pMDG2 and psPAX2) and switched to inactivated high-serum (30%) medium. At 24- and 48-h posttransfection, supernatants were collected, pooled, spun, and filtered to eliminate residual cells. Cas9-expressing HeLa cells were then infected with 200 to 300 μL virus together with polybrene; at 24-h postinfection, they were selected with puromycin (1.5 μg/mL) for at least 48 h. LRRC8A KO clones were obtained by single-cell sorting in 96-well plates on FACSAria Fusion (Becton Dickinson). After clonal expansion, clones were checked by Western blot for the presence of LRRC8A protein. LRRC8A KO clone 6 was used to generate cell lines expressing LRRC8A-WT and LRRC8A-S217A under an inducible promoter following the transfection protocol described by Kowarz and colleagues (60). Briefly, cells were seeded in 6-well plates and transfected the following day with Lipofectamine 3000 (Invitrogene) using pSB100X transposase plasmid and pSBtet-BN constructs with the LRRC8A WT and mutants described in this work. At 24-h post-transfection, cells were selected with up to 5,000 μg/mL G418 (Sigma) for up to 1 wk. Induction was determined using a range of doxycycline (Sigma) concentrations (from 10 to 250 ng/mL), and protein levels were analyzed from cell extracts by Western blot.

Cell Transfection. Cells were transfected with 1 mg/mL polyethylenimine (PEI, Polysciences, 23966) (PEI:DNA ratio of 5:1) diluted in 150 mM NaCl (for patch-clamp studies of MSK1 activation of LRRC8A, YFP quenching, and MSK1 imaging) or with Lipofectamine 3000 (Invitrogen) when transfected with WNK1 mutants, siLRRC8A, or siRNA-resistant LRRC8A-WT or LRRC8A-S217A in KD cells. A ratio of 1:1 LIPO:DNA diluted in Opti-MEM (Gibco) was used, following manufacturer's instructions. All experiments were performed between 24- and 36-h posttransfection, except for patch-clamp experiments, which were carried out in KD cells overexpressing an siRNA-resistant channel, which were performed between 48- and 72-h posttransfection.

Generation of Constructs. MSK1 putative phosphorylation sites in LRRC8A were mutated on the pIRES2-EGFP construct (gift from the Patapoutian laboratory; note that the LRRC8A sequence has two siRNA resistance regions) using the Q5 site-directed mutagenesis kit (NEB), following the manufacturer's instructions. NEBaseChanger software was used for oligonucleotide design (*SI Appendix*, Table S2). The ICL fragments (amino acids F144 to D258) from WT or mutated LRRC8A pIRES2-EGFP plasmids were cloned into *Eco*RI/*Not*I sites of the pGEX-6P-1 plasmid for bacterial expression by PCR amplification. Full-length WT LRRC8A or S217A mutant were cloned into EcoRI/NotI sites of pGEX-6P-1 plasmid by PCR amplification with a forward oligonucleotide containing the myc tag after the EcoRI restriction site. MSK1 was subcloned from MSK1-BioID2-HA plasmid (a gift from R. Gomis, Institute for Research in Biomedicine [IRB], Barcelona) into the EcoRI

site of pGEX-6P-1 plasmid for GST purification or PCR amplified and cloned into *Not*I/*Nco*I sites of the pETM11 plasmid for His-tag purification. Constructs with LRRC8A under an inducible promoter were generated by PCR amplification from the corresponding pIRES-EGFP plasmids with a reverse oligonucleotide carrying the CRISPR resistance nucleotide changes against the guide SC GD2 and cloned into the *Sfi*I site of the pSB-BN plasmid. The pEBG-FLAG-WNK1 L369F L371F construct was generated by substituting the *Mre*I-*Bsu*36I region from the pcDNA5 FRT/TO FLAG WNK1 L369F L371F into the pEBG-FLAG- WNK1 Wt plasmid.

Cell Viability Assays. Cells were seeded into 6-well plates and then challenged with the indicated NaCl concentration on the following day. After 24 h, supernatants and cells were collected, pelleted, washed in phosphate-buffered saline (PBS), and then stained with 1 μg/mL PI (Sigma). PI staining was assessed by flow cytometry in FACSCalibur using CellQuest software (Becton Dickinson). LRRC8A KO cells expressing WT or mutant LRRC8A under an inducible promoter were seeded in 12-well plates with doxycycline and were challenged with the indicated NaCl concentration on the following day. After 24 h, supernatants and cells were collected, pelleted, washed with PBS, and stained with 1 μg/mL PI. PI staining was assessed by flow cytometry in Gallios (Beckman Coulter), and profiles were generated by using FlowJo software. Alternatively, after 24 to 48 h of stress, plates were washed with PBS, fixed, and stained with crystal violet solution for 20 min at room temperature (RT), rinsed with water, and air dried. Viable cells attached to the plate stained with crystal violet, making the intensity of the staining directly proportional to cell viability.

Protein Purification. Recombinant GST proteins were expressed in *Escherichia coli* BL21 cells grown at 37 °C to an optical density (wavelength of 600nm) (OD600) of 0.5 for ICL-LRRC8A and MSK1 and of 0.8 for full-length LRRC8A proteins. GST-tagged proteins were induced for 3 h by adding 1 mM IPTG and switching the culture temperature to 25 °C. After induction, cells were collected by centrifugation and resuspended in a 1/50 volume of STET 1× buffer (100 mM NaCl, 10 mM Tris · HCl pH 8.0, 10 mM ethylenediaminetetraacetic acid [EDTA] pH 8.0, 5% Triton X-100 supplemented with 2 mM DTT, 1 mM phenylmethylsulfonyl fluoride [PMSF], 1 mM benzamidine, 200 mg/mL leupeptin, and 200 mg/mL pepstatin). Cells were lysed by brief ice-cold sonication and cleared by high-speed centrifugation. GST-fused proteins were pulled down from supernatants with 300 μL Glutathione-Sepharose beads (GE Healthcare, 50% slurry equilibrated with STET) by mixing for 45 min at 4 °C. The Glutathione-Sepharose beads were collected by brief centrifugation and washed first four times in STET buffer and then four times in 50 mM Tris · HCl pH 8.0 buffer supplemented with 2 mM DTT. GST-fused proteins were eluted in 500 μL (for ICL-LRRC8A and MSK1) or 200 μL (for full-length LRRC8A) 50 mM Tris · HCl pH 8.0 buffer supplemented with 2 mM DTT and 10 mM reduced glutathione (Sigma) by mixing for 30 min at 4 °C.

His-MSK1 was expressed in *E. coli* BL21 cells grown at 37 °C until they reached an OD600 of 0.5, followed by 3 h of induction with 1 mM IPTG at 25 °C. After induction, cells were collected by centrifugation and resuspended in sonication buffer (20 mM Tris pH 8, 100 mM NaCl, 1 mM PMSF, 1 mM benzamidine, 2 μg/mL leupeptin, and 2 μg/mL pepstatin). Cells were lysed by brief ice-cold sonication and cleared by high-speed centrifugation. His-MSK1 was pulled down from the supernatant with 300 μL TALON Metal Affinity resin (Clontech) and equilibrated with sonication buffer by mixing for 45 min at 4 °C. The TALON Metal Affinity resins were collected by brief centrifugation and washed six times with sonication buffer. The His-MSK1 was eluted in 300 μL elution buffer (20 mM Tris · HCl pH 8.0, 100 mM NaCl, and 50 mM imidazole) by mixing for 30 min at 4 °C.

In Vitro Kinase Assay. GST-MSK1 or His-MSK1 was activated in vitro in 1× kinase assay buffer (50 mM Tris · HCl pH 7.5, 10 mM $MgCl_2$, and 2 mM DTT) with 100 μM cold ATP for 30 min at 37 °C. This activated GST-MSK1 or His-MSK1 was used to phosphorylate eluted GST-fused proteins in vitro. The reactions were carried out in 1× kinase assay buffer in the presence of 1 μCi/assay of radiolabeled 32P-γ-ATP (3000 Ci/mmol, Perkin-Elmer) in a final volume of 40 μL/assay for 30 min at 37 °C. Reactions were stopped by adding SB 5× (250 mM Tris · HCl pH 6.8, 0.5 M DTT, 10% sodium dodecyl sulfate [SDS], 20% glycerol, and 0.5% bromophenol blue) and boiling at 95 °C for 5 min. Phosphorylated proteins were subjected to SDS-polyacrylamide gel electrophoresis (PAGE) and blotted onto a polyvinylidene difluoride (PVDF) membrane, which was exposed to KODAK BIOMAX XAR films or a phosphorimager.

In Vivo LRRC8A Phosphorylation Assays. HeLa cells were seeded in 10-cm dishes. After 1 d, they were stressed with 100 mM NaCl for 15 min with or without a 1-h pretreatment with 10 μM MSK1 inhibitor SB747651A (Tocris) dissolved in DMSO. Cell extracts were collected with 1× Laemmli buffer (2% SDS) supplemented with PhosSTOP (Roche) and protease inhibitors and briefly sonicated to reduce viscosity. Samples were run on an 8% PAGE gel supplemented with 50 μM Phos-tag (Wako) and 20 μM $MnCl_2$ for 2 h at 30 mA in the cold. Proteins were transferred onto a PVDF membrane for 2 h at 300 mA on ice. LRRC8A mobility shift was detected by incubating the membranes with LRRC8A monoclonal antibody (Sigma), and signals were detected with ECL Clarity reagent (Bio Rad).

Western Blotting. After the indicated treatments, cells were washed with ice-cold PBS and scraped into 300 μL lysis buffer (10 mM Tris · HCL pH 7.5, 1% Nonidet P-40, 2 mM EDTA, 50 mM NaF, 50 mM b-glycerophosphate, 1 mM sodium vanadate, supplemented with the protease inhibitors 1 mM PMSF, 1 mM benzamidine, 200 μg/mL leupeptin, and 200 μg/mL pepstatin). Lysates were cleared by centrifugation. Samples were resolved using SDS-PAGE and then blotted onto a PDVF membrane. Following incubation of the blots with the indicated antibodies, signals were detected using the ECL detection reagent (Amersham).

Patch-Clamp Experiments. Whole-cell recordings were obtained as previously described (50) using an Axon 200A amplifier (Axon Instruments). Currents were acquired at 33 kHz and filtered at 1 kHz. The pClamp8 software (Axon Instruments) was used for pulse generation, data acquisition, and subsequent analysis. LRRC8A-like chloride currents were measured in cells clamped at 0 mV and pulsed for 400 ms from −100 mV to +100 mV in 50-mV steps every 30 s. I_{Cl}^- whole-cell currents were measured using pipettes (2 to 3 MΩ) filled with a solution containing 100 mM *N*-methyl-D-glucamine chloride ($NMDGCl^-$), 1.2 mM $MgCl_2$, 1 mM EGTA, 10 mM Hepes, 2 mM Na_2ATP, and 0.5 mM Na_3GTP (pH 7.3 and 300 mOsm/l). To achieve a controlled intracellular IS of 0.08, 78.2 mM NaCl was used instead of $NMDGCl^-$ and adjusted osmolarity to ∼410 mOsm/l. The external solution contained $NMDGCl^-$ at 100 mM (for iso- and hypotonic conditions) or 185 mM (hypertonic conditions), 0.5 mM $MgCl_2$, 5 mM KCl, 1.8 mM $CaCl_2$, 5 mM glucose, and 10 mM Hepes, pH 7.4. Osmolarity was adjusted to 310 (isotonic), 220 (hypotonic), or 415 (hypertonic) mOsm/l with mannitol.

YFP and Chloride Imaging. Cells grown in coverslips and transiently transfected with halide-sensitive YFP constructs (37) were washed thoroughly with isotonic solution containing 110 mM NaCl, 5 mM KCl, 1.8 mM $CaCl_2$, 0.5 mM $MgCl_2$, 5 mM glucose, 10 mM Hepes, pH 7.4. Osmolarity was adjusted to 310 mOsm/l with 80 mM mannitol. The hypotonic solution (220 mOsm/l) contained 85 mM NaCl and no mannitol, while the hypertonic solution (410 mOsm/l) contained 185 mM NaCl or NaI. For YFP-NKCC1 imaging experiments, hypertonic solutions were prepared by adding 100 mOsm of mannitol (410 mOsm/l) to an isotonic solution in order to avoid changes in ionic concentrations that could affect the sensor. Video microscopic measurements of YFP fluorescence were obtained using an Olympus IX70 inverted microscope with a 20× or 40× oil-immersion objective. The excitation light (488 nm) was supplied by a Polychrome IV monochromator (Till Photonics) and directed toward the cells under study by a 505DR dichromatic mirror (Omega Optical). Fluorescence images were collected by a digital charge-coupled device camera (Hamamatsu Photonics) after passing through a 535DF emission filter (Omega Optical) using AquaCosmos software (Hamamatsu Photonics). Images of basal fluorescence levels in isotonic solution were computed every 5 s and recorded for 2 min, followed by exposure to either 30% hypo- or hypertonic solutions for 5 or 10 min, respectively. After this, 80 μL 200 mM NaI was added to induce YFP quenching (adapted from ref. 23). Alternatively, instead of a NaI buffer, a hypertonic NaCl solution was substituted for an equivalent solution containing an equimolar concentration of NaI. The YFP signal was normalized to 1 (set at 100% of YFP fluorescence) at 5 s before NaI addition. The percentage of fluorescence decay after NaI addition was calculated as the YFP quenching response.

Recordings of relative changes in intracellular $[Cl^-]$ were carried out in cells loaded with 5 mM *N*-(6-methoxyquinolyl)acetoethyl ester (MQAE) (61) for 60 min at 37 °C or in cells transfected with the ratiometric Cl^- sensor ClopHensor. For MQAE experiments, cells were excited at 360 nm and emission was collected at >515 nm. Photobleaching correction of the normalized MQAE signal was performed when necessary. For experiments using the ClopHensor, fluorescent images were collected using a Leica laser-scanning confocal inverted microscope TCS Sp5 with a 40× oil-immersion objective. Cyan channel fluorescence was excited at 458 nm using an Argon laser and detected from 500 to 550 nm, and the red channel was excited using an He-Ne laser at 561 nm and detected from 600 to 700 nm. Laser scanning was performed using 400 Hz line frequency, 512 × 512 pixel format, and pinhole aperture set at 2 AU. Images were taken every 30 s using 3-line average. HeLa cells were monitored in iso for 2.5 min, treated with

hypertonic solution for 10 min, and calibrated with 0 and 120 mM [Cl^-] in the presence of the Cl^-/OH^- ionophore exchanger tributyltinchloride (10 μM) and the K^+/H^+ exchanger nigericin (5 μM) (TBTN). Calibration of ClopH sensor was performed in vivo. Cells ($n = 7$) were monitored in isotonic solution for 2.5 min and then perfused with standard solutions at 0, 15, 30, 50, 80, 110, and 120 mM [Cl^-] for 4 min in the presence of TBTN. All calibration solutions contained 120 mM [K^+] 20 mM [Na^+], 1 mM Mg gluconate, 1 mM Ca gluconate, 5 mM glucose and 10 mM Hepes, pH 7.3 and 300 mOsm/l. The desired [Cl^-] in each standard solution was achieved by a combination of Na and K gluconate replacing NaCl and KCl. Cyan-to-red ratio of fluorescence intensity was normalized to isotonic treatment and expressed as mean ± SEM.

Cell Volume Measurements. One confluent T75 flask was used for each volume measurement experiment. When needed, drug preincubations were performed on detached cells inside the cell incubator for the indicated time. All volume measurements were performed at RT, keeping the cells in warm complete medium. A Z2 Coulter Counter Analyzer (Beckmann) was used to measure the volumes of the cell populations. Each sample taken by the counter contained between 20,000 and 100,000 cells in a volume of 100 or 500 μL. Three baseline measures were taken in normal (isotonic) medium before adding the hypertonic or hypotonic medium. Changes in cell volume were normalized to basal volumes. To calculate the percentage of RVD or RVI, the Δ of mean basal volume was calculated to the volume at each time point. Maximum (swollen cells) or minimum (shrunken cells) cell volume changes were set as 100% and subsequent values were referred to this maximum/minimun to calculate the percentage of recovery (%RVI) (62).

Immunoprecipitation of WNK1 and Phospho-WNK1. One or two 100-mm plates of cells at maximum confluency were used for each immunoprecipitation. Medium was exchanged for isotonic solution for at least 5 min. Then, the solution was exchanged to perform the desired treatment (hypo- to isotonic or hypertonic) for the indicated time. Isotonic solutions were maintained for controls. Solutions were gently removed, and 250 to 300 μL ice-cold lysis buffer (50 mM Tris/HCl, pH 7.5, 1 mM EGTA, 1 mM EDTA, 50 mM sodium fluoride, 5 mM sodium pyrophosphate, 1 mM sodium orthovanadate, 1% [wt/vol] Nonidet P-40, 0.27 M sucrose, 0.1% [vol/vol] 2-mercaptoethanol, and protease inhibitors [1 tablet per 50 mL]) containing 1× PhosSTOP (Sigma) were added to each plate. Cells (on ice) were scraped thoroughly. Cell lysates were clarified by a 15-min centrifugation at 26,000 *g* and at 4 °C. For immunoprecipitation (IP), 1 mL supernatant (~2 mg of protein) was transferred to a new tube, and 12 μg anti-WNK1 antibody was added. For anti–phospho-WNK IP, 12 μg anti-phospho antibody plus 10 μg dephosphorylated form of the phosphopeptide antigen were added to cell lysates. IPs were incubated overnight at 4 °C under continuous rotation. Additional 25 μL aliquots cleared cell lysates were kept as inputs for Western blot analysis when needed. On the following day, 40 μL (50% slurry) protein-G-Sepharose beads (previously blocked overnight with 1% bovine serum albumin) were added to each IP and incubated for 2.5 h at 4 °C under continuous rotation. Immunoprecipitates were washed three times with 1 mL lysis buffer containing 0.15 M NaCl and 1× PhosSTOP and twice with 1 mL buffer A (50 mM Tris/HCl, pH 7.5, and 0.1 mM EGTA). Bound proteins were eluted in 40 μL 1× lithium dodecyl sulfate sample buffer containing 1× reducing agent (Invitrogen) and heated at 70 °C for 10 min. Eluted samples were subjected to electrophoresis on precast NuPAGE 3 to 8% Tris Acetate gels (Invitrogen) and transferred to nitrocellulose membranes. Membranes were blocked in 1× Tris-buffered saline 0.05% tween 20 containing 10% nonfat dried milk powder. For the total-WNK1 condition, IPs were divided and loaded into two separate wells in the same gel to obtain both total- and phospho-WNK1 bands and thus the ratio of the two signals (phospho/total). For the phospho-WNK1 condition, the ratio to total-WNK1 signal was calculated using the total-WNK1 band obtained from the inputs. Primary antibodies were incubated overnight at 4 °C and secondary antibodies for 1 h at RT. Bands were developed with ECL substrate Clarity using the ChemiDoc XRS+ system and quantified with Quantity One Software (BioRad).

Statistical Analysis. All electrophysiological, imaging, cell volume, and biochemical data are presented as mean ± SEM. Statistical analyses were performed using SigmaPlot software. First, a normality test was run, and for the data that followed normal distributions, a Student's paired or unpaired *t* test was applied between two groups and one-way ANOVA followed by Bonferroni or Dunnett post hoc tests across multiple groups. In the case of multiple groups, comparison of different conditions to a control group is run using the Dunnett's method, whereas all pairwise comparisons were evaluated using Bonferroni's method or one-way ANOVA followed by Holm–Sidak post hoc test, as suggested by the statistical package. For the data that did not assume Gaussian distributions, a Mann–Whitney *U* test was used for comparing two groups. The criterion for statistically significant difference was $P < 0.05$. Statistical analyses of data generated with the genetic screening were performed using bash and R scripts; visualizations were done using the ggplot2 (v3.1.0) (63) and ggrepel (v0.8.0) (64) R packages.

Data Availability. Gene data generated in this study have been uploaded to Gene Expression Omnibus under accession number GSE158316. The code generated for this study is available at GitHub (https://github.com/CellSignaling/SWELL1_HeLa_CRISPR_screening_2020).

ACKNOWLEDGMENTS. We thank Dr. R. Gomis (IRB Barcelona) and Drs. A. Patapoutian (Scripps Research, US) and L. Galietta (Naples University, Italy) for reagents. P.S. is a recipient of an FPU (formación de profesorado universitario) fellowship (FPU16/05114). R.A. was a recipient of a Marie Curie Cofund Programme fellowship (EU). P.L. was a recipient of a personal investigator predoctoral fellowship (Generalitat de Catalunya). R.B. was a recipient of a Juan de la Cierva fellowship. G.S. was supported by an Advanced Postdoc. Mobility fellowship (P300P3_147895) by the Swiss National Science Foundation. This work was supported by grants from the Ministry of Science, Innovation, and Universities (PGC2018-094136-B-I00 to F.P.; BFU2017-85152-P and Fondo Europeo de Desarrollo Regional [FEDER] to E.d.N.; RTI2018-099718-B-I00 and FEDER to M.A.V.), the Catalan Government (2017 SGR 799), the Fundación Botín, and the Banco Santander through its Santander Universities Global Division to F.P. We gratefully acknowledge institutional funding from the Ministry of Science, Innovation and Universities through the Centres of Excellence Severo Ochoa Award and from the Centres de Recerca de Catalunya (CERCA) Programme of the Catalan Government and the Unidad de Excelencia María de Maeztu, funded by the Agencia Estatal de Investigación (AEI) (CEX2018-000792-M). F.P. and E.d.N. are recipients of an Institució Catalana de Recerca i Estudis Avançats (ICREA) Acadèmia award (Generalitat de Catalunya).

1. E. K. Hoffmann, I. H. Lambert, S. F. Pedersen, Physiology of cell volume regulation in vertebrates. *Physiol. Rev.* **89**, 193–277 (2009).
2. M. B. Burg, J. D. Ferraris, N. I. Dmitrieva, Cellular response to hyperosmotic stresses. *Physiol. Rev.* **87**, 1441–1474 (2007).
3. F. Lang *et al*., Functional significance of cell volume regulatory mechanisms. *Physiol. Rev.* **78**, 247–306 (1998).
4. X. Escoté, M. Zapater, J. Clotet, F. Posas, Hog1 mediates cell-cycle arrest in G1 phase by the dual targeting of Sic1. *Nat. Cell Biol.* **6**, 997–1002 (2004).
5. A. Gubern *et al*., The N-terminal phosphorylation of RB by p38 bypasses its inactivation by CDKs and prevents proliferation in cancer cells. *Mol. Cell* **64**, 25–36 (2016).
6. A. Duch *et al*., Coordinated control of replication and transcription by a SAPK protects genomic integrity. *Nature* **493**, 116–119 (2013).
7. E. de Nadal, G. Ammerer, F. Posas, Controlling gene expression in response to stress. *Nat. Rev. Genet.* **12**, 833–845 (2011).
8. R. Amat *et al*., Rapid reversible changes in compartments and local chromatin organization revealed by hyperosmotic shock. *Genome Res.* **29**, 18–28 (2019).
9. M. L. McManus, K. B. Churchwell, K. Strange, Regulation of cell volume in health and disease. *N. Engl. J. Med.* **333**, 1260–1266 (1995).
10. H. Pasantes-Morales, Channels and volume changes in the life and death of the cell. *Mol. Pharmacol.* **90**, 358–370 (2016).
11. C. D. Bortner, J. A. Cidlowski, Absence of volume regulatory mechanisms contributes to the rapid activation of apoptosis in thymocytes. *Am. J. Physiol.* **271**, C950–C961 (1996).
12. C. Levinson, Regulatory volume increase in Ehrlich ascites tumor cells. *Biochim. Biophys. Acta* **1021**, 1–8 (1990).
13. J. A. O'Brien, R. J. Walters, M. A. Valverde, F. V. Sepúlveda, Regulatory volume increase after hypertonicity- or vasoactive-intestinal-peptide-induced cell-volume decrease in small-intestinal crypts is dependent on Na(+)-K(+)-2Cl- cotransport. *Pflugers Arch.* **423**, 67–73 (1993).
14. J. M. Russell, Sodium-potassium-chloride cotransport. *Physiol. Rev.* **80**, 211–276 (2000).
15. G. E. Breitwieser, A. A. Altamirano, J. M. Russell, Osmotic stimulation of Na(+)-K(+)-Cl- cotransport in squid giant axon is [Cl-]i dependent. *Am. J. Physiol.* **258**, C749–C753 (1990).
16. C. Lytle, B. Forbush, Regulatory phosphorylation of the secretory Na-K-Cl cotransporter: Modulation by cytoplasmic Cl. *Am. J. Physiol.* **270**, C437–C448 (1996).
17. A. Zagórska *et al*., Regulation of activity and localization of the WNK1 protein kinase by hyperosmotic stress. *J. Cell Biol.* **176**, 89–100 (2007).
18. A. T. Piala *et al*., Chloride sensing by WNK1 involves inhibition of autophosphorylation. *Sci. Signal.* **7**, ra41 (2014).
19. B. F. X. Dowd, B. Forbush, PASK (proline-alanine-rich STE20-related kinase), a regulatory kinase of the Na-K-Cl cotransporter (NKCC1). *J. Biol. Chem.* **278**, 27347–27353 (2003).
20. A. C. Vitari *et al*., Functional interactions of the SPAK/OSR1 kinases with their upstream activator WNK1 and downstream substrate NKCC1. *Biochem. J.* **397**, 223–231 (2006).

21. S. Grinstein, C. A. Clarke, A. Rothstein, Activation of Na+/H+ exchange in lymphocytes by osmotically induced volume changes and by cytoplasmic acidification. *J. Gen. Physiol.* **82**, 619–638 (1983).
22. M. A. Valverde *et al*., The multidrug resistance P-glycoprotein modulates cell regulatory volume decrease. *EMBO J.* **15**, 4460–4468 (1996).
23. T. D. Bond, S. Ambikapathy, S. Mohammad, M. A. Valverde, Osmosensitive C1- currents and their relevance to regulatory volume decrease in human intestinal T84 cells: Outwardly vs. inwardly rectifying currents. *J. Physiol.* **511**, 45–54 (1998).
24. E. Vázquez, M. Nobles, M. A. Valverde, Defective regulatory volume decrease in human cystic fibrosis tracheal cells because of altered regulation of intermediate conductance Ca2+-dependent potassium channels. *Proc. Natl. Acad. Sci. U.S.A.* **98**, 5329–5334 (2001).
25. J. M. Fernández-Fernández, M. Nobles, A. Currid, E. Vázquez, M. A. Valverde, Maxi K+ channel mediates regulatory volume decrease response in a human bronchial epithelial cell line. *Am. J. Physiol. Cell Physiol.* **283**, C1705–C1714 (2002).
26. P. de los Heros, D. Pacheco-Alvarez, G. Gamba, Role of WNK kinases in the modulation of cell volume. *Curr. Top Membr.* **81**, 207–235 (2018).
27. R. Akella *et al*., Osmosensing by WNK kinases. *Mol. Biol. Cell* 10.1091/mbc.E20-01-0089 (2021).
28. T. Hart *et al*., High-resolution CRISPR screens reveal fitness genes and genotype-specific cancer liabilities. *Cell* **163**, 1515–1526 (2015).
29. Z. Qiu *et al*., SWELL1, a plasma membrane protein, is an essential component of volume-regulated anion channel. *Cell* **157**, 447–458 (2014).
30. F. K. Voss *et al*., Identification of LRRC8 heteromers as an essential component of the volume-regulated anion channel VRAC. *Science* **344**, 634–638 (2014).
31. N. Decher *et al*., DCPIB is a novel selective blocker of $I_{Cl,swell}$ and prevents swelling-induced shortening of Guinea-pig atrial action potential duration. *Br. J. Pharmacol.* **134**, 1467–1479 (2001).
32. C. L. Cannon, S. Basavappa, K. Strange, Intracellular ionic strength regulates the volume sensitivity of a swelling-activated anion channel. *Am. J. Physiol.* **275**, C416–C422 (1998).
33. T. Voets, G. Droogmans, G. Raskin, J. Eggermont, B. Nilius, Reduced intracellular ionic strength as the initial trigger for activation of endothelial volume-regulated anion channels. *Proc. Natl. Acad. Sci. U.S.A.* **96**, 5298–5303 (1999).
34. R. Syeda *et al*., LRRC8 proteins form volume-regulated anion channels that sense ionic strength. *Cell* **164**, 499–511 (2016).
35. M. Díaz, M. A. Valverde, C. F. Higgins, C. Rucăreanu, F. V. Sepúlveda, Volume-activated chloride channels in HeLa cells are blocked by verapamil and dideoxyforskolin. *Pflugers Arch.* **422**, 347–353 (1993).
36. M. A. Valverde, G. M. Mintenig, F. V. Sepúlveda, Differential effects of tamoxifen and I- on three distinguishable chloride currents activated in T84 intestinal cells. *Pflugers Arch.* **425**, 552–554 (1993).
37. L. J. Galietta, P. M. Haggie, A. S. Verkman, Green fluorescent protein-based halide indicators with improved chloride and iodide affinities. *FEBS Lett.* **499**, 220–224 (2001).
38. J. Han, J. D. Lee, L. Bibbs, R. J. Ulevitch, A MAP kinase targeted by endotoxin and hyperosmolarity in mammalian cells. *Science* **265**, 808–811 (1994).
39. A. Cuenda *et al*., SB 203580 is a specific inhibitor of a MAP kinase homologue which is stimulated by cellular stresses and interleukin-1. *FEBS Lett.* **364**, 229–233 (1995).
40. M. Deak, A. D. Clifton, L. M. Lucocq, D. R. Alessi, Mitogen- and stress-activated protein kinase-1 (MSK1) is directly activated by MAPK and SAPK2/p38, and may mediate activation of CREB. *EMBO J.* **17**, 4426–4441 (1998).
41. S. Naqvi *et al*., Characterization of the cellular action of the MSK inhibitor SB-747651A. *Biochem. J.* **441**, 347–357 (2012).
42. C. E. McCoy *et al*., Identification of novel phosphorylation sites in MSK1 by precursor ion scanning MS. *Biochem. J.* **402**, 491–501 (2007).
43. C. Lytle, B. Forbush, The Na-K-Cl Cotransport Protein of Shark Rectal Gland 11. Regulation by direct phosphorylation. *J. Biol. Chem.* **267**, 25438–25443 (1992).
44. M. Haas, D. McBrayer, C. Lytle, [Cl-]i-dependent phosphorylation of the Na-K-Cl cotransport protein of dog tracheal epithelial cells. *J. Biol. Chem.* **270**, 28955–28961 (1995).
45. A. Currid, B. Ortega, M. A. Valverde, Chloride secretion in a morphologically differentiated human colonic cell line that expresses the epithelial Na+ channel. *J. Physiol.* **555**, 241–250 (2004).
46. M. Pedersen, M. Carmosino, B. Forbush, Intramolecular and intermolecular fluorescence resonance energy transfer in fluorescent protein-tagged Na-K-Cl cotransporter (NKCC1): Sensitivity to regulatory conformational change and cell volume. *J. Biol. Chem.* **283**, 2663–2674 (2008).
47. K. Piechotta, J. Lu, E. Delpire, Cation chloride cotransporters interact with the stress-related kinases Ste20-related proline-alanine-rich kinase (SPAK) and oxidative stress response 1 (OSR1). *J. Biol. Chem.* **277**, 50812–50819 (2002).
48. D. Arosio *et al*., Simultaneous intracellular chloride and pH measurements using a GFP-based sensor. *Nat. Methods* **7**, 516–518 (2010).
49. P. Li *et al*., LRRC8 family proteins within lysosomes regulate cellular osmoregulation and enhance cell survival to multiple physiological stresses. *Proc. Natl. Acad. Sci. U.S.A.* **117**, 29155–29165 (2020).
50. M. A. Valverde *et al*., Volume-regulated chloride channels associated with the human multidrug-resistance P-glycoprotein. *Nature* **355**, 830–833 (1992).
51. D. R. Gill *et al*., Separation of drug transport and chloride channel functions of the human multidrug resistance P-glycoprotein. *Cell* **71**, 23–32 (1992).
52. T. Bond, S. Basavappa, M. Christensen, K. Strange, ATP dependence of the ICl,swell channel varies with rate of cell swelling. Evidence for two modes of channel activation. *J. Gen. Physiol.* **113**, 441–456 (1999).
53. M. Shekarabi *et al*., WNK kinase signaling in ion homeostasis and human disease. *Cell Metab.* **25**, 285–299 (2017).
54. E. Lang *et al*., Accelerated apoptotic death and in vivo turnover of erythrocytes in mice lacking functional mitogen- and stress-activated kinase MSK1/2. *Sci. Rep.* **5**, 17316 (2015).
55. K. Karelina *et al*., Mitogen and stress-activated kinases 1/2 regulate ischemia-induced hippocampal progenitor cell proliferation and neurogenesis. *Neuroscience* **285**, 292–302 (2015).
56. W. Li *et al*., MAGeCK enables robust identification of essential genes from genome-scale CRISPR/Cas9 knockout screens. *Genome Biol.* **15**, 554 (2014).
57. A. Subramanian *et al*., Gene set enrichment analysis: A knowledge-based approach for interpreting genome-wide expression profiles. *Proc. Natl. Acad. Sci. U.S.A.* **102**, 15545–15550 (2005).
58. B. Langmead, C. Trapnell, M. Pop, S. L. Salzberg, Ultrafast and memory-efficient alignment of short DNA sequences to the human genome. *Genome Biol.* **10**, R25 (2009).
59. A. Liberzon *et al*., Molecular signatures database (MSigDB) 3.0. *Bioinformatics* **27**, 1739–1740 (2011).
60. E. Kowarz, D. Löscher, R. Marschalek, Optimized Sleeping Beauty transposons rapidly generate stable transgenic cell lines. *Biotechnol. J.* **10**, 647–653 (2015).
61. A. S. Verkman, M. C. Sellers, A. C. Chao, T. Leung, R. Ketcham, Synthesis and characterization of improved chloride-sensitive fluorescent indicators for biological applications. *Anal. Biochem.* **178**, 355–361 (1989).
62. J. M. Fernandez-Fernandez, M. Nobles, A. Currid, E. Vazquez, M. A. Valverde, Maxi K+ channel mediates regulatory volume decrease response in a human bronchial epithelial cell line. *Am. J. Physiol. Cell Physiol.* **283**, C1705–C1714 (2002).
63. H. Wickham, *Gggplot2: Elegant Graphics for Data Analysis* (Springer New York LLC, New York, 2016).
64. K. Slowikowski, Automatically Position Non-Overlapping Text Labels with, "ggplot2" (Version 0.8.2, R package ggrepel). https://cran.r-project.org/web/packages/ggrepel/index.html. Accessed 9 September 2020.